Clinical Cancer Research

Mesothelin-Targeted Thorium-227 Conjugate (MSLN-TTC): Preclinical Evaluation of a New Targeted Alpha Therapy for Mesothelin-Positive Cancers

Urs B. Hagemann[1], Christine Ellingsen[2], Joachim Schuhmacher[3], Alexander Kristian[2], Anne Mobergslien[2], Véronique Cruciani[2], Katrine Wickstroem[2], Christoph A. Schatz[1], Christoph Kneip[1], Sven Golfier[1], Roger Smeets[2], Steinar Uran[2], Hartwig Hennekes[1], Jenny Karlsson[2], Roger M. Bjerke[2], Olav B. Ryan[2], Dominik Mumberg[1], Karl Ziegelbauer[1], and Alan S. Cuthbertson[2]

Abstract

Purpose: Targeted thorium-227 conjugates (TTC) represent a new class of molecules for targeted alpha therapy (TAT). Covalent attachment of a 3,2-HOPO chelator to an antibody enables specific complexation and delivery of the alpha particle emitter thorium-227 to tumor cells. Because of the high energy and short penetration range, TAT efficiently induces double-strand DNA breaks (DSB) preferentially in the tumor cell with limited damage to the surrounding tissue. We present herein the preclinical evaluation of a mesothelin (MSLN)-targeted thorium-227 conjugate, BAY 2287411. MSLN is a GPI-anchored membrane glycoprotein overexpressed in mesothelioma, ovarian, pancreatic, lung, and breast cancers with limited expression in healthy tissue.

Experimental Design: The binding activity and radiostability of BAY 2287411 were confirmed bioanalytically. The mode-of-action and antitumor potency of BAY 2287411 were investigated *in vitro* and *in vivo* in cell line and patient-derived xenograft models of breast, colorectal, lung, ovarian, and pancreatic cancer.

Results: BAY 2287411 induced DSBs, apoptotic markers, and oxidative stress, leading to reduced cellular viability. Furthermore, upregulation of immunogenic cell death markers was observed. BAY 2287411 was well-tolerated and demonstrated significant antitumor efficacy when administered via single or multiple dosing regimens *in vivo*. In addition, significant survival benefit was observed in a disseminated lung cancer model. Biodistribution studies showed specific uptake and retention of BAY 2287411 in tumors and enabled the development of a mechanistic pharmacokinetic/pharmacodynamic model to describe the preclinical data.

Conclusions: These promising preclinical results supported the transition of BAY 2287411 into a clinical phase I program in mesothelioma and ovarian cancer patients (NCT03507452).

Introduction

Targeted alpha therapy (TAT) holds great potential for the treatment of cancer based on the specific delivery of alpha-particle emitting radionuclides to tumors (1). Following the worldwide marketing authorization of the first-in-class TAT Xofigo (radium-223 dichloride) for the treatment of mCRPC (2), there has been an increased interest in new applications of TAT. The inherent bone-seeking accumulation of radium-223 (3) allows for effective delivery to bone metastases, but the lack of suitable chelating agents has hindered the development of radioimmunoconjugates using this radionuclide. On the other hand, the progenitor of radium-223, thorium-227, can be directly complexed at ambient temperature to antibody conjugates bearing chelators of the octadentate 3,2-hydroxypyridinone (3,2-HOPO) class (4, 5). Fortuitously, the half-life of thorium-227 (18.7 days) is compatible with the blood half-life of therapeutic antibodies in humans, the decay chain resulting in the generation of a total of five high-energy alpha and two beta particles ending with the nonradioactive element lead-207 (6).

We have recently described the generation of targeted thorium-227 conjugates (TTC) and evaluated their potencies in *in vitro* and *in vivo* models of acute myeloid leukemia (7) and in models of renal cell carcinoma (8). The mode-of-action (MoA) of TTCs is predominantly linked to the robust induction of irreparable double-strand DNA breaks (9). Unlike antibody drug conjugates (ADC), due to the high energy and short path length (2–10 cell diameters) of the alpha particles (10), TTCs are not strictly dependent on antigen internalization and may obviate the development of cellular resistance.

Mesothelin (MSLN) is a 40-kDa GPI-anchored membrane glycoprotein, and it has been proposed to play a role in mediating

[1]Bayer AG, Berlin, Germany. [2]Bayer AS, Oslo, Norway. [3]Bayer AG, Wuppertal, Germany.

Note: Supplementary data for this article are available at Clinical Cancer Research Online (http://clincancerres.aacrjournals.org/).

Corresponding Author: Urs B. Hagemann, Bayer AG, Muellerstrasse 178, 13342 Berlin, Germany. Phone: 49 30 468194864; E-mail: urs.hagemann@bayer.com

Clin Cancer Res 2019;25:4723–34

doi: 10.1158/1078-0432.CCR-18-3476

Translational Relevance

Mesothelin (MSLN)-targeted thorium-227 conjugate (BAY 2287411) is the first targeted alpha therapy (TAT) being developed for the treatment of patients suffering from MSLN-positive solid tumors. BAY 2287411 induces irreparable double-strand DNA breaks upon alpha decay by thorium-227, resulting in cell death. In cell line and patient-derived xenograft models, BAY 2287411 demonstrated specific, single-dose antitumor activity correlating with mesothelin expression levels and was independent of tumor tissue origin. BAY 2287411 is able to overcome intratumoral heterogeneous target expression often limiting the efficacy of therapeutic agents *in vivo*. Without any reported cellular resistance mechanisms to TAT, BAY 2287411 also has the potential to evade the ones affecting existing therapies. On the basis of the promising preclinical results, BAY 2287411 has advanced into a phase I clinical trial in patients with mesothelioma and ovarian cancer (NCT03507452).

cell–cell adhesion and metastatic spread through the involvement of CA125 and the metalloproteinase MMP-7 (11–13). Under physiologic conditions, MSLN expression is confined to the peritoneal and pleural cavities and pericardium. In cancers, overexpression of MSLN has been reported in a wide range of solid cancers such as mesothelioma, ovarian, pancreatic, lung, and breast cancers (14). MSLN knockout mice exhibit normal development, reproduction, and blood cell count (11). The extracellular domain of MSLN has been demonstrated to bind to mucin glycoprotein CA125. Intracellularly, MSLN can activate NFκB, MAPK, and PI3K signaling pathways, thereby promoting cell proliferation and resistance to apoptosis (15). The restricted expression of MSLN on healthy tissues, combined with the high expression on several solid cancers renders it an attractive tumor antigen for targeted cancer therapy and several preclinical and clinical approaches are currently being pursued including CAR-T cells, vaccines, antibodies (amatuximab), recombinant immunotoxins (SS1P, and RG7787) as well as antibody drug conjugates (anetumab ravtansine/BAY 94-9343; aMSLN-MMAE (h7D9.v3), and MDX-1204 (14, 16–18).

We present herein the preclinical evaluation of BAY 2287411, a MSLN-targeting thorium-227 conjugate (MSLN-TTC), which is based on the fully human IgG1 antibody BAY 86-1903 (anetumab) covalently attached to a thorium-227 complexing 3,2-HOPO chelator (4, 5). BAY 2287411 demonstrated potent *in vitro* and *in vivo* activity in cellular and patient-derived xenograft (PDX) models of breast, lung (mesothelioma), ovarian, and pancreatic cancer. Furthermore, using a mechanistic pharmacokinetic/pharmacodynamic model, we were able to fit and accurately describe the preclinical *in vivo* data.

Materials and Methods

Compounds, cell lines, and animals

The MSLN-targeting antibody BAY 86-1903, the MSLN-TTC BAY 2287411, the radiolabeled isotype control BAY 2473626, the non-radiolabeled MSLN antibody-chelator conjugate BAY 2287409, and the radionuclide thorium-227 were manufactured by Bayer AS. The vehicle used in all studies was 30 mmol/L citrate, 70 mmol/L NaCl, 0.5 mg/mL PABA, 2 mmol/L EDTA, pH 5.5, supplemented with 0.1 mg/mL IgG2a-κ from murine myeloma (#M7769, Sigma-Aldrich).

The OVCAR-3, UWB1.289 and UWB1.289+*BRCA1* (19), EKVX, AsPC-1, Capan-2, NCI-H322, BxPC-3, HCT-116, and Kato III cells were obtained from ATCC and DSMZ between 2010 and 2016 and authenticated using short tandem repeat DNA fingerprinting at Leibniz Institute (German Collection of Micro-organisms and Cell Cultures, DSMZ) before the experiments. HT29-MSLN cells were generated as described previously (17). NCI-H226-*luc* cells are MSLN-expressing cells that have been genetically transfected with the luciferase gene (17).

All animal experiments were performed under the respective national animal welfare laws in Norway, Germany, Denmark, and Finland and approved by the local authorities.

Synthesis and characterization of BAY 2287411

The fully human anti-mesothelin mAb anetumab BAY 86-1903 was expressed, harvested, and purified as described previously (17). The MSLN antibody-chelator conjugate BAY 2287409 was prepared by coupling an N-hydroxysuccinimide-activated 3,2-hydroxypyridinone (HOPO) chelator covalently to the ε-amino groups of the lysine residues of BAY 86-1903 as described previously (7). The chelator-to-antibody ratio (CAR) for the prepared batch of BAY 2287409 was 0.5. Hence, BAY 2287409 is a mixture of MSLN antibody-chelator conjugate and MSLN antibody BAY 86-1903.

BAY 2287409 was radiolabeled with thorium-227 in 30 mmol/L citrate, 70 mmol/L NaCl, 0.5 mg/mL PABA, 2 mmol/L EDTA, pH 5.5 at room temperature for 20 to 30 minutes, resulting in BAY 2287411. Radioactivity concentrations varied between 1 and 2 MBq/mL.

BAY 2287411 was analyzed for radiostability over the course of 48 hours by HPLC and the immunoreactive fraction (IRF) was determined as described by Lindmo (20) and detailed in the Supplementary Information. The binding affinity of BAY 2287411 to recombinant human MSLN was determined with an ELISA assay as described in the Supplementary Information.

A radiolabeled isotype control BAY 2473626 was prepared similarly to BAY 2287411.

Cytotoxicity and mode-of-action of BAY 2287411

In vitro cytotoxicity experiments were performed in 12 cell lines with various MSLN expression levels (338–242,000 detected antibodies bound per cell as determined by flow cytometry analysis, Supplementary Table S1) using CellTiter-Glo assay (Promega) after a 5-day exposure to BAY 2287411 as described in the Supplementary Information.

To study the proposed MoA of BAY 2287411, OVCAR-3 cells as well as the isogenic cell line pair UWB1.289 and UWB1.289+BRCA1 were treated with BAY 2287411 and analyzed for induction of double-strand DNA breaks by measuring the percentage of phosphorylated histone protein γ-H2AX positive cells. OVCAR-3 and/or HT29-MSLN cells were further analyzed for expression of danger-associated molecular patterns (DAMP), for cell-cycle phase by staining cells with PI RNAse, and for release of apoptosis markers with cleaved caspase-3/7-Glo Kit (Promega), ROS-Glo H_2O_2 Kit (Promega) and RealTime-Glo Annexin V Apoptosis and Necrosis assay (Promega) or stained for *in vitro* immunofluorescence analysis. Details are described in the Supplementary Information.

In vivo efficacy and biodistribution of BAY 2287411

In vivo efficacy and biodistribution of BAY 2287411 were assessed in cell line–derived xenograft (CDX) models of colorectal (HT29-MSLN), ovarian (OVCAR-3), pancreatic (BxPC-3, Capan-2), lung (NCI-H226-*luc*), and in PDX models of ovarian (ST103) and breast (ST2185B) cancer in mice. The mice were treated with a single intravenous injection of BAY 2287411 with doses ranging from 100 to 500 kBq/kg. Pharmacokinetic studies were performed in BxPC-3, Capan-2, HT29-MSLN, OVCAR-3, ST103, and ST2185B models by harvesting tumor, blood, femurs, and/or organs at time points between 0.5 hour and 28 days after dosing. Samples were analyzed for remaining radioactivity with high purity germanium gamma detector (HPGe) in *ex vivo* samples and expressed as percentage of injected dose per gram (% ID/g) as described in the Supplementary Information. Unless mentioned otherwise, BAY 2287411 and radiolabeled isotype control BAY 2473626 were administered at a fixed total antibody dose of 0.14 mg/kg, and additionally, effects of changes in total antibody dose were tested by varying doses between 0.029 and 0.75 mg/kg. In all studies, the mice were predosed with 200 μg of IgG2a-κ from murine myeloma (#M7769, Sigma-Aldrich) prior to TTC treatment. Tumor growth was determined as tumor volumes measured by caliper. In the NCI-H226-*luc* model, tumor growth was measured by bioluminescence imaging (BLI). Details of all *in vivo* studies are provided in Supplementary Information.

The disseminated NCI-H226-luc model was performed at Bayer AS, the HT29-MSLN with mixed ratios at Bayer AG, the OVCAR-3 study at Pharmatest Services Ltd, the HT29-MSLN and the Capan-2 study at Biotest Facility, and studies with PDX models ST103 and ST2185B at Minerva Imaging ApS.

IHC was performed on xenograft tumor tissues as described in Supplementary Information.

Pharmacokinetic/pharmacodynamic modeling

A mechanistic pharmacokinetic/pharmacodynamic model was developed to describe the biodistribution and efficacy of BAY 2287411 and to determine the impact of total antibody dose on the tumor uptake/efficacy in preclinical models as described in the Supplementary Information.

Statistical analysis

All analyses of the *in vivo* efficacy of BAY 2287411 were performed using the statistical programming language R (version 3.4.3). Validity of the model assumptions was checked for each fitted statistical model. Analyses were performed using linear models estimated with generalized least squares that included separate variance parameters for each study group. Mean comparisons between the treatment and control groups were performed using the estimated linear model. Statistical analysis for NCI-H2226-*luc* dissemination model survival data was performed using the Cox proportional hazards regression.

Results

Preparation and characterization of BAY 2287411

The MSLN-TTC BAY 2287411 (Fig. 1A) was prepared by conjugation of the 3,2-HOPO-chelator via amide bond formation to lysine side-chain amino groups on the MSLN-targeted fully human IgG1 antibody BAY 86-1903 and subsequent radiolabeling with thorium-227. Binding of BAY 86-1903, MSLN antibody-chelator conjugate BAY 2287409, and BAY 2287411 was shown to be specific for MSLN as determined by ELISA (Fig. 1B). Neither conjugation nor radiolabeling affected the binding properties. BAY 2287411 was shown to remain intact and retain its binding potency over the course of 48 h upon storage at room temperature with an median IRF value of 77%.

In vitro potency of BAY 2287411

The MoA of BAY 2287411 was explored in MSLN-positive cell lines. Using OVCAR-3 cells, it was demonstrated that BAY 2287411 induced double-strand DNA breaks (Fig. 1C) and caused G_2–M cell-cycle arrest (Fig. 1D), resulting in reduced cell viability (Fig. 1E). *In vitro* cytotoxicity experiments were conducted in 12 MSLN-positive cancer cell lines of various tissue origins (mesothelioma, ovarian, pancreas, colorectal, lung, and gastric) that differed in surface expression levels of MSLN (Supplementary Table S1; Supplementary Fig. S1). Dependency on target density was observed as evidenced by the decrease in the ratio of IC_{50} values for the radiolabeled isotype control BAY 2473626 compared with BAY 2287411 which correlated well with decreased MSLN expression level on the cell lines studied (Supplementary Table S1). No reduction of cell viability was observed when cells where incubated in the presence of non-radiolabeled MSLN antibody-chelator conjugate BAY 2287409.

The sensitizing impact of BAY 2287411 on cells harboring homologous recombination repair deficiency, for example, *BRCA1* deletion, was further investigated in the human ovarian cancer isogenic cell line pair UWB1.289/UWB1.289+*BRCA1* (19). Increased levels of γH2AX, indicating double-strand DNA breaks, were observed in the BAY 2287411–treated *BRCA1*-deficient UWB1.289 cells compared to the UWB1.289+*BRCA1* cells (Supplementary Fig. S1C). The increase was concomitant with a 2-fold increase in IC_{50} value (Supplementary Fig. S1D; Supplementary Table S1).

Irradiation of cancer cells by TAT may evoke multiple pathways and cellular responses ultimately resulting in cytotoxicity (21). We therefore evaluated whether the observed cytotoxicity induces the apoptotic pathway. A dose-dependent induction of caspase-3 activity was observed in BAY 2287411-treated HT29-MSLN and OVCAR-3 cells compared with untreated cells (Supplementary Fig. S2A and S2B). Despite the complete abolishment of the caspase-3 activity by the pan-caspase inhibitor Z-VAD-FMK, BAY 2287411–treated cells still showed a major decrease in cell viability (Supplementary Fig. S2C and S2D). Furthermore, using immunofluorescence, release of cytochrome C into the cytoplasm, a central event in apoptosis (22, 23), was observed in BAY 2287411–treated cells (Supplementary Fig. S2E). These data demonstrate induction of classical markers of apoptotic cell death by BAY 2287411; however, inhibition of the pathway does not rescue cells.

Ionizing radiation leads to oxidizing events, for example, via products of water radiolysis such as reactive oxygen species (ROS; ref. 24). Indeed, an increase of ROS was observed in BAY 2287411–treated OVCAR-3 and HT29-MSLN cells compared with untreated cells (Supplementary Fig. S3A and S3B). In an experiment determining the ability of BAY 2287411 to induce necrosis (21), a 2-fold increase in necrotic signal was observed in BAY 2287411–treated cells in comparison with untreated cells. The necrotic signal was not decreased in the presence of necrosis inhibitor necrostatin-1 (Supplementary Fig. S3C; ref. 25). An

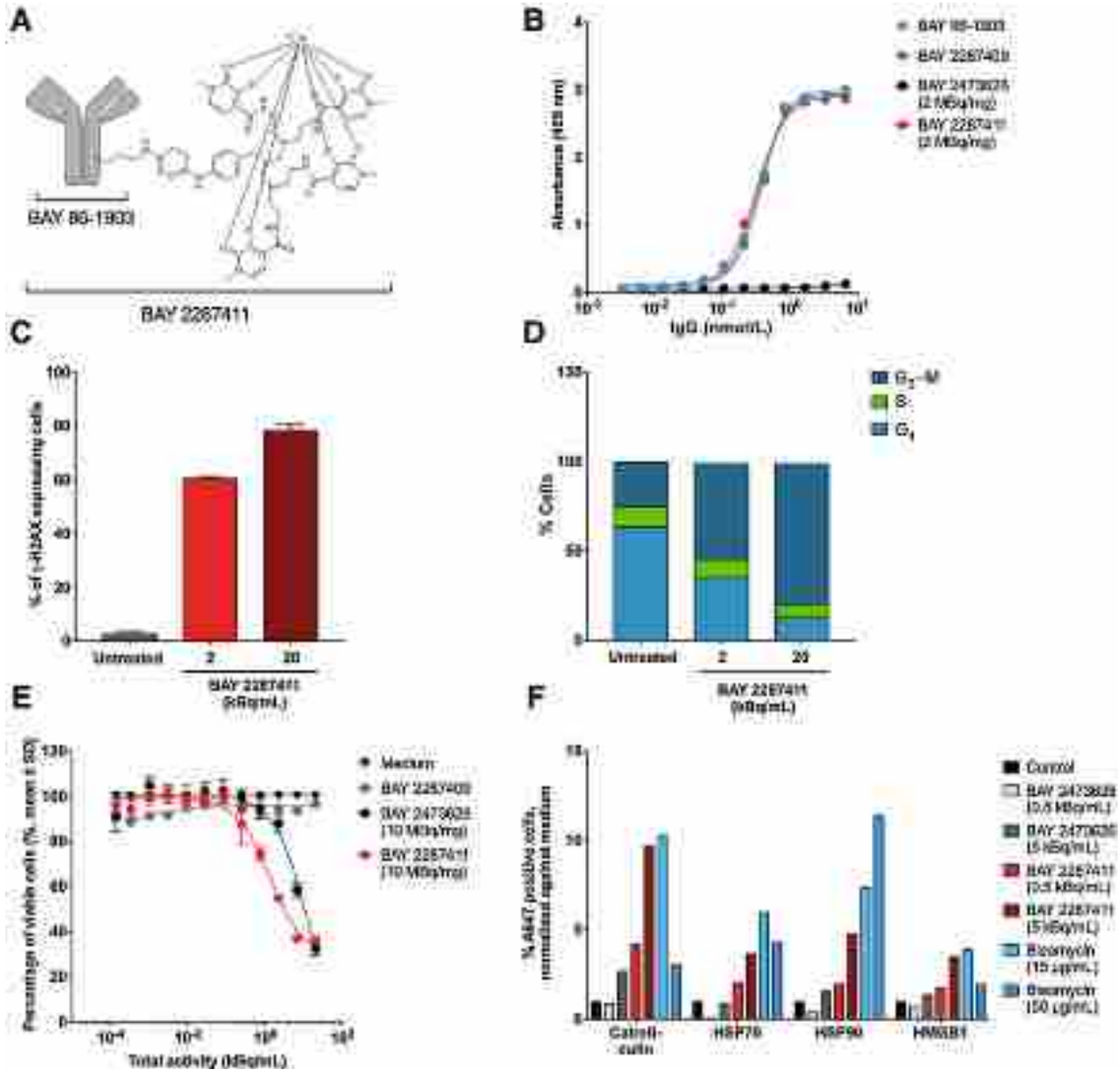

Figure 1.

Structure and binding of MSLN-TTC BAY 2287411 and its *in vitro* characterization upon exposure on OVCAR-3 cells. Non-radiolabeled MSLN antibody–chelator conjugate BAY 2287409 and radiolabeled isotype control BAY 2473626 were used as controls. **A,** Structure of MSLN-TTC BAY 2287411, consisting of the antibody BAY 86-1903, covalently attached to the 3,2-HOPO chelator enabling complexation of thorium-227. **B,** Binding of MSLN antibody BAY 86-1903, non-radiolabeled MSLN antibody–chelator conjugate BAY 2287409, radiolabeled BAY 2287411, and radiolabeled isotype control BAY 2473626 to human recombinant MSLN as determined by ELISA. **C,** Induction of double-strand DNA breaks by exposure of OVCAR-3 cells to BAY 2287411 as determined by detection of γ-H2AX protein. **D,** Cell-cycle analysis of OVCAR-3 cells after treatment with BAY 2287411. **E,** Viability of OVCAR-3 cells after treatment with BAY 2287411, BAY 2287409, and BAY 2473626. **F,** Induction of DAMPs on the cell surface membrane by BAY 2287411 in comparison with BAY 2473626 and bleomycin on live cells as analyzed by flow cytometry.

immunofluorescence analysis supported the finding (Supplementary Fig. S3D).

The ability of BAY 2287411 to induce the upregulation of DAMP markers, the hallmark of immunogenic cell death, was investigated in OVCAR-3 cells. The membrane-localized DAMPs calreticulin, HSP70, HSP90, and HMGB1, were detected by flow cytometry analysis in cells after exposure to BAY 2287411 (Fig. 1F). BAY 2287411 specifically induced upregulation of all DAMP markers on OVCAR-3 cells to similar levels as the positive control bleomycin (26). Additional studies are planned for evaluating the potential immuno-stimulatory effect of BAY 2287411 in immunocompetent mouse animal models.

Biodistribution of BAY 2287411 in xenograft models

The biodistribution of BAY 2287411 (single dose, 500 kBq/kg, total antibody dose 0.14 mg/kg) was studied in CDX and PDX models. The models expressed MSLN at various levels ranging from 4,200 to 242,413 antibodies bound per cell as determined by flow cytometry and IHC (Table 1). Significant retention in tumors over the 4-week study period (672 hours; 28 days) was observed and tumor accumulation of BAY 2287411 was shown to

Table 1. Summary of *in vivo* efficacy of BAY 2287411 in correlation to MSLN expression levels

Model, cancer type (mutational status where applicable[a])	Antibodies bound per cell[b]	Percentage of cells staining at intensity 0/1/2/3[c]	H-score	Treatment/control ratio[d]		
				100 or 125 kBq/kg	250 kBq/kg	500 kBq/kg
HT29-MSLN, colorectal cancer (*APC*^{E853}, *BRAF*^{V600E,T119S}, *PIK3CA*^{P449T}, *TP53*^{R273H}, *WRN*^{L1255})	242,413	5.1/6.5/8.2/80.2	264	1.3 (n.s.)	**0.38**[e]	**0.09**[e]
ST103, ovarian cancer PDX (*BRCA*^{del})	192,000[f]	9.6/13.9/40.3/36.2	203	**0.46**[g] (125 kBq/kg) **0.05**[e] (4× 125 kBq/kg)	**0.05**[e] (250 kBq/kg) 0.28 (n.s.) (2× 250 kBq/kg)	**0.02**[e]
ST2185B, breast cancer PDX	181,000[f]	7.5/18.1/50.4/24	191	0.62 (n.s.) (125 kBq/kg) **0.19**[e] (4× 125 kBq/kg)	**0.38**[e] (250 kBq/kg) **0.07**[e] (2× 250 kBq/kg)	**0.1**[e]
Capan-2, pancreatic cancer (*FANCC*^{E52*}, *KRAS*^{G12V})	18,000	34.9/28.3/25/12	114	**0.36**[e] (125 kBq/kg) **0.07**[e] (4× 125 kBq/kg)	**0.16**[e] (250 kBq/kg) **0.13**[e] (2× 250 kBq/kg)	**0.26**[e]
OVCAR-3, ovarian cancer (*TP53*^{R248Q})	37,877	38.8/34.9/22.7/3.6	101	NA	**0.083**[e] (ab 0.14 mg/kg) **0.077**[e] (ab 0.75 mg/kg)	NA
BxPC-3, pancreatic cancer (*CDK10*^{S293L}, *ERCC2*^{R156}, *ERCC6*^{I422F}, *TP53*^{Y220C})	4,200	63/28.3/7.1/1.7	48	0.69 (n.s.)	0.37 (n.s.)	**0.39**[g]
NCI-H226-*luc*, intravenous model of lung cancer	183,411	37.2/57.4/5.1/0.3	69	**0.11**[e]	**0.01**[e]	**0.002**[e]

NOTE: Statistical analysis was performed using linear models estimated with generalized least squares that included separate variance parameters for each study group. Mean comparisons between the treatment and control groups were performed using the estimated linear model.

Abbreviations: ND, not detected; NA, not available; n.s., nonsignificant

[a]See refs. 42 and 43.

[b]Determined using flow cytometry.

[c]IHC score based on an experiment using a SP74 antibody. 0, not detected; 1, low; 2, medium; 3, high.

[d]Tumor volume measured by caliber for all models except for NCI-H226-*luc* models by bioluminescence imaging.

[e]$P < 0.001$.

[f]Determined theoretically by extrapolation using HT29-MSLN xenograft values.

[g]$P < 0.05$.

be specific when compared with the radiolabeled isotype control BAY 2473626 (Supplementary Fig. S4). BAY 2287411 showed a typical blood clearance profile for antibodies being cleared from blood over 3 to 7 days (Supplementary Fig. S4). MSLN expression levels were assessed in parallel by IHC (Supplementary Fig. S5), and it was observed that tumor uptake tended to correlate with MSLN expression levels. The highest accumulation was observed in the transfected CDX model HT29-MSLN and in the PDX models ST103 and ST2185B. These models were determined to have H-scores of 264, 203, and 191, respectively, and were therefore considered as MSLN-high expressing models. In these models, thorium-227 uptake increased over the time period of 3 to 7 days as blood levels dropped below detectable limits with a measured accumulation close to 100% ID/g at 672 hours (ST103). In contrast, thorium-227 accumulation was in the range of 28% ID/g in the Capan-2 model and around approximately 22% ID/g in the BxPC-3 model. These models had MSLN expression levels with H-scores of 114 (Capan-2) and 48 (BxPC-3), respectively, and were therefore considered to be medium to low-MSLN expressing models.

In vivo efficacy of BAY 2287411 in cell line and patient-derived xenograft models

In vivo efficacy of BAY 2287411 was assessed in CDX and PDX models of colon, ovarian, pancreatic, and breast cancer. BAY 2287411 was administered at varying radioactivity doses using a fixed total antibody dose of 0.14 mg/kg.

Dose-dependent tumor growth regressions were observed in the high MSLN-expressing models HT29-MSLN (colorectal cancer, CDX), ST103 (ovarian cancer, PDX), and ST2185B (breast cancer, PDX) with treatment/control (T/C) ratios of 0.09, 0.02, and 0.1, respectively, at the highest radioactivity dose of 500 kBq/kg (Fig. 2A–C; Table 1). Non-radiolabeled antibody-chelator conjugate BAY 2287409 showed no tumor growth inhibition. Treatment with BAY 2287411 resulted in induction of double-strand DNA breaks as evidenced by IHC detection of γ-H2AX protein in HT29-MSLN and Capan-2 tumors treated with BAY 2287411 at the doses indicated, isolated at the end of the study (Supplementary Figs. S6 and S7). In models of medium MSLN expression (OVCAR-3 ovarian cancer and Capan-2 pancreatic cancer CDX), BAY 2287411 also demonstrated significant antitumor activity (Fig. 2D and E; Table 1) while in the low-expressing model BxPC-3, tumor stasis was observed (Fig. 2F; Table 1). These results suggest that efficacy increased concomitantly with the tumor accumulation and retention of BAY 2287411 is driven by the MSLN expression levels (Supplementary Fig. S5; Table 1).

Furthermore, it was investigated whether BAY 2287411 administered on a weekly basis for 4 weeks resulted in the same *in vivo* efficacy as a single equivalent dose of radioactivity. As presented in Fig. 2B, C, E, and G–I (Table 1), BAY 2287411 administered at a dose of 2× 250 or 4× 125 kBq/kg resulted in significant antitumor efficacy equivalent at the end of the study to the 500 kBq/kg single dose. However, in comparison with the single dose of 500 kBq/kg, the growth response was slower due to the increased time required to accumulate an effective dose of radioactivity in the tumors. We also evaluated in the Capan-2 xenograft whether there is a change in MSLN expression levels upon multiple administration of BAY 2287411. As presented in tumors treated with BAY 2287411 at 1× 500 kBq/kg or 4× 125 kBq/kg (Supplementary Fig. S7),

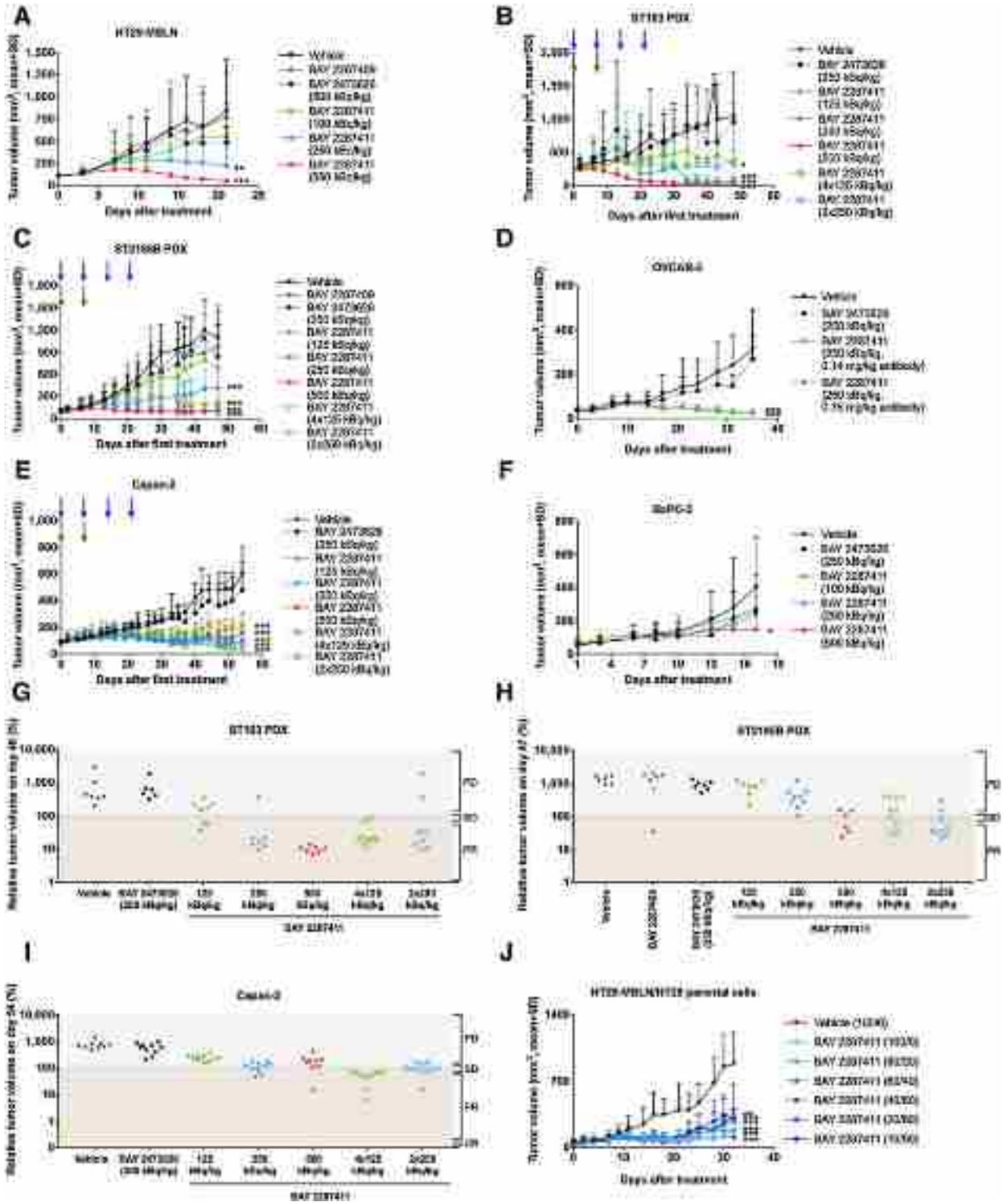

Figure 2.

In vivo efficacy of MSLN-TTC BAY 2287411 in various cell line and patient-derived xenograft models in mice. Radiolabeled isotype control BAY 2473626 and/or non-radiolabeled MSLN antibody–chelator conjugate BAY 2287409 were used as controls. TTCs were administered at a total antibody dose of 0.14 mg/kg unless indicated otherwise. **A,** Growth curves of HT29-MSLN colorectal tumors in mice treated with vehicle, a single dose of BAY 2287411 (100, 250, or 500 kBq/kg, i.v.), BAY 2473626 (500 kBq/kg, i.v), or BAY 2287409 (i.v.). **B,** Growth curves of ST103 ovarian cancer PDX tumors in mice treated with vehicle, BAY 2287411 (a single dose of 125, 250, or 500 kBq/kg; or 2× 250 kBq/kg; or 4× 125 kBq/kg, i.v.), or BAY 2473626 (250 kBq/kg, i.v). (*Continued on the following page.*)

MSLN expression was still detectable at similar levels to vehicle-treated animals at study end.

Heterogeneous intratumoral antigen expression often hampers the efficacy of targeted therapies such as ADCs. The ability of the alpha-emitter thorium-227 to penetrate 2 to 10 cell layers (10) and its independence of antigen internalization may allow BAY 2287411 to be active in patients with heterogeneous MSLN-target expression. In an attempt to study potential bystander and cross-fire effects, in combination with tumor target heterogeneity, a CDX model was established using MSLN-overexpressing transfected HT29-MSLN cells spiked with increasing proportions of MSLN-negative parental HT29 cells as shown in Fig. 2J and Supplementary Fig. S8. In this experiment, a single dose of 500 kBq/kg BAY 2287411 resulted in significant tumor growth inhibition in all groups tested. Surprisingly, even the tumors inoculated with only 10% and 20% MSLN-positive cells demonstrated a robust and significant response compared with the vehicle control group. As expected, the most pronounced antitumor activity (as defined by lower T/C ratios) was observed in the groups with highest percentage of MSLN-transfected cells (Supplementary Fig. S8).

The *in vivo* efficacy of BAY 2287411 was further confirmed in a disseminated model of lung cancer using the luciferase-transfected cell line NCI-H226. BAY 2287411 was found to be efficacious at all doses tested (100, 250, and 500 kBq/kg; with T/C ratios of 0.11, 0.01 and 0.002, respectively), which also translated to an increased survival probability in the treatment groups compared with the vehicle (Fig. 3A–C; Table 1). The observed benefit was 17 days (median) for radiolabeled isotype control BAY 2473626 and between 30 and 84 days for MSLN-TTC BAY 2287411 ($P < 0.001$ for BAY 2287411 doses 100 and 250 kBq/kg) compared with vehicle group. The most pronounced effect was for the 500 kBq/kg dose where all animals survived to end of study (Fig. 3C; Supplementary Table S2).

In all studies presented, BAY 2287411 was well-tolerated as evidenced by no measurable body weight loss greater than 10% in any of the *in vivo* models. Dose-dependent, reversible suppression of white blood cells was observed in the Capan-2 model when BAY 2287411 was applied at doses of 250, 2× 250, 4× 125, and 500 kBq/kg compared with vehicle. However, no significant differences were observed in the relative numbers of cells between the varying doses of BAY 2287411 (Supplementary Fig. S9).

Mechanistic pharmacokinetic/pharmacodynamic model to describe observed *in vivo* efficacy and to predict the dependence on total antibody dose

Having conducted the xenograft studies described above, we further used these data to (i) describe the pharmacokinetic/pharmacodynamic of BAY 2287411, (ii) calculate the cumulative hits per tumor cell, (iii) determine the potency parameter of thorium-227 (k2), and (iv) evaluate the influence of the total antibody dose on the cumulative hits per tumor cell in correlation with the MSLN receptor density. To start, a mechanistic pharmacokinetic/pharmacodynamic model to describe pharmacokinetics and pharmacodynamics of BAY 22787411 and receptor turnover in tumors *in vivo* was developed (Fig. 4A). The model was applied to quantitatively describe concentration/time (c/t)-profiles of thorium-227 activity in blood and tumor as well as tumor growth inhibition in various cell line xenograft models (HT29-MSLN, OVCAR-3, Capan-2, BxPC-3, and NCI-H226) and in the PDX models ST103 and ST2185B. As presented in Fig. 4B and C, the c/t profile of BAY 2287411 in blood and tumor in the biodistribution study using the HT29-MSLN model could be described at high precision. Furthermore, using the pharmacokinetic/pharmacodynamic model, we were able to simulate the observed efficacy in the HT29-MSLN model at high accuracy (Fig. 4D).

The model was further used to calculate the cumulative hits per tumor cell, the tumor static concentration (TSC) and the potency parameter (k2), linking the thorium-227 activity in tumor to the effect observed (Table 2). TSC increased with decreasing tumor doubling time from 840 Bq/mL (Capan-2, tumor doubling time: ∼21 days) to 4,000 Bq/mL (OVCAR-3 and HT29-MSLN tumor doubling times: ∼6.9 and 3 days), corresponding to 8 to 36 cumulative hits/cell. These values are in line with the published data, suggesting that approximate five hits per tumor cell are lethal *in vitro* (27, 28). Furthermore, the calculations indicate that the therapeutic effective dose in xenograft models depends on the tumor doubling times. In addition, k2 was determined to be about 2×10^{-6} mL/Bq/h and, as such, to be independent of the receptor density and tissue origin.

The model was further used to predict the cumulative hits/tumor cell as a function of the total antibody dose, ranging from 0.029 to 0.75 mg/kg, in dependence of the target density (range of 5,000–1,000,000 receptors/cell) at a fixed radioactivity dose (Fig. 4E). A steep decrease of cumulative hits per tumor cell at increasing total antibody doses and decreasing target densities

(*Continued.*) The multiple dosings were administered as depicted by the green (2× 250 kBq/kg) or blue (4× 125 kBq/kg) arrows. **C,** Growth curves of ST2185B breast cancer PDX tumors in mice treated with vehicle, BAY 2287411 (a single dose of 125, 250, or 500 kBq/kg; or 2× 250 kBq/kg; or 4× 125 kBq/kg, i.v.), BAY 2473626 (250 kBq/kg, i.v), or BAY 2287409 (i.v.). The multiple dosings were administered as depicted by the green (2× 250 kBq/kg) or blue (4× 125 kBq/kg) arrows. **D,** Growth curves of OVCAR-3 ovarian tumors in mice treated with vehicle, BAY 2287411 (a single dose of 250 kBq/kg, i.v.), or BAY 2473626 (250 kBq/kg, i.v.) at a total antibody dose of 0.14 mg/kg or 0.75 mg/kg. **E,** Growth curves of Capan-2 pancreatic tumors treated with vehicle, BAY 2287411 (a single dose of 125, 250, or 500 kBq/kg; or 2× 250 kBq/kg; or 4× 125 kBq/kg, i.v.), or BAY 2473626 (250 kBq/kg, i.v). The multiple dosings were administered as depicted by the green (2× 250 kBq/kg) or blue (4× 125 kBq/kg) arrows. **F,** Growth curves of BxPC-3 pancreatic tumors treated with vehicle or a single dose of BAY 2287411 (100, 250, or 500 kBq/kg, i.v.), or BAY 2473626 (500 kBq/kg, i.v). **G,** Relative tumor volumes of ST103 ovarian cancer PDX tumors in mice treated with vehicle, BAY 2287411 (a single dose of 125, 250, or 500 kBq/kg; or 2× 250 kBq/kg; or 4× 125 kBq/kg, i.v.), or radiolabeled isotype control BAY 2473626 (250 kBq/kg, i.v) as described in **B**. **H,** Relative tumor volumes of ST2185B breast cancer PDX tumors in mice treated with vehicle, BAY 2287411 (a single dose of 125, 250, or 500 kBq/kg; or 2× 250 kBq/kg; or 4× 125 kBq/kg, i.v.), BAY 2473626 (250 kBq/kg, i.v), or BAY 2287409 (i.v.) as described in **C**. **I,** Relative tumor volumes of Capan-2 pancreatic tumors treated with vehicle, BAY 2287411 (a single dose of 125, 250, or 500 kBq/kg; or 2× 250 kBq/kg; or 4× 125 kBq/kg, i.v.), or BAY 2473626 (250 kBq/kg, i.v) as described in **E**. **J,** Growth curves of tumors in mice inoculated with varying ratios between MSLN-transfected HT29-MSLN colorectal cancer cells in mixture with parental HT29 colorectal cancer cells. Mice were treated with vehicle or a single dose of BAY 2287411 (500 kBq/kg, i.v.). PD, progressive disease; SD, stable disease; PR, partial response; CR, complete response. Statistical analysis was performed using linear models estimated with generalized least squares that included separate variance parameters for each study group. Mean comparisons between the treatment and vehicle groups were performed using the estimated linear model. *, $P < 0.05$; **, $P < 0.01$; ***, $P < 0.001$.

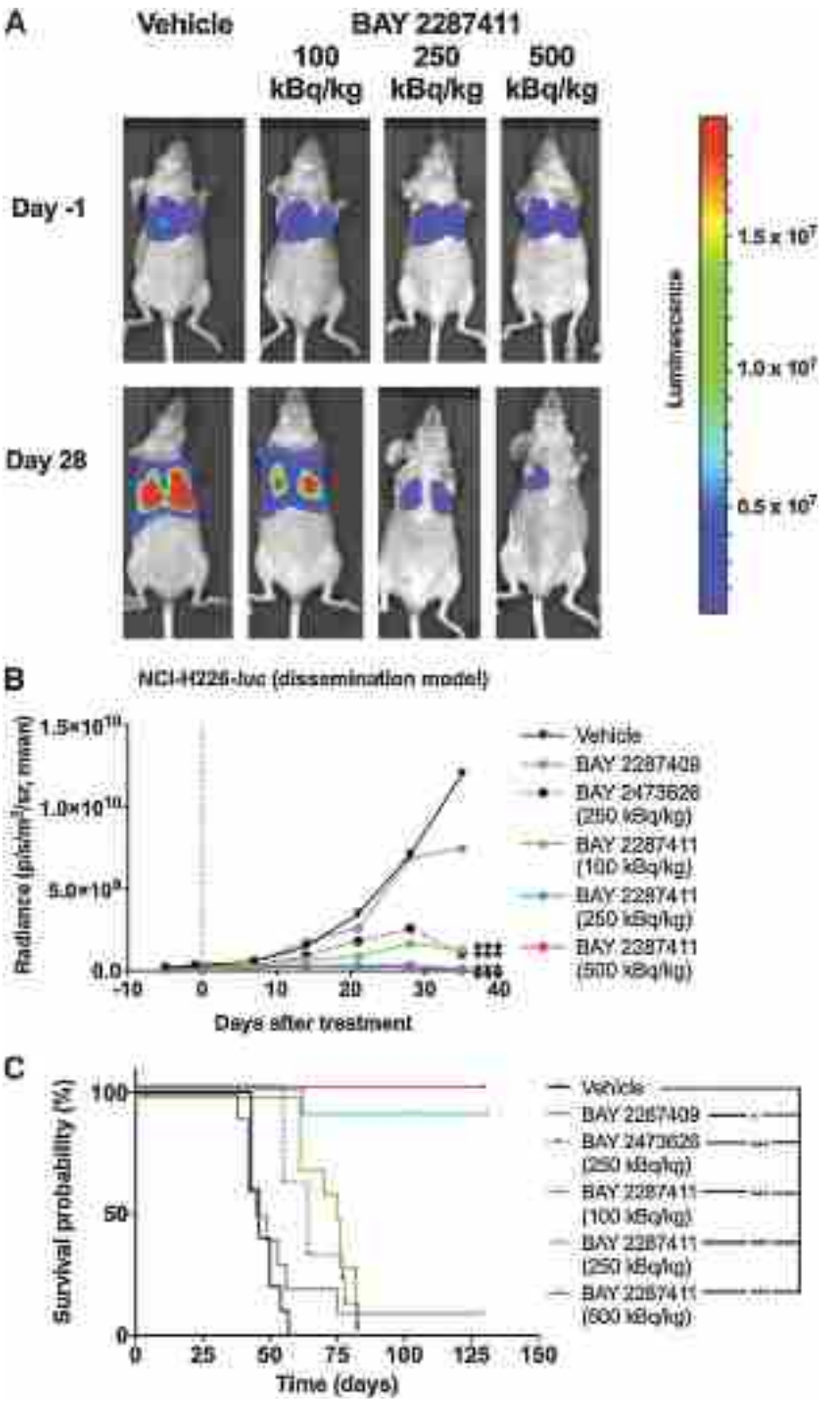

Figure 3.

In vivo efficacy of MSLN-TTC BAY 2287411 in intravenously inoculated NCI-H226-*luc* lung cancer model. The mice were treated with vehicle or a single dose of BAY 2287411 (100, 250, or 500 kBq/kg, i.v.), radiolabeled isotype control BAY 2473626 (250 kBq/kg, i.v.), or non-radiolabeled MSLN antibody–chelator conjugate BAY 2287409 (i.v.) at a total antibody dose of 0.14 mg/kg. **A,** Representative images of total tumor burden as measured by BLI. **B,** Tumor growth curves as measured by BLI. **C,** Survival analysis of mice carrying NCI-H226-*luc* tumors. Statistical analysis was performed using Cox proportional hazards regression. *, $P < 0.05$; **, $P < 0.01$; ***, $P < 0.001$.

was expected due to target saturation. However, a total antibody dose of 0.14 mg/kg can be expected to maintain exposure and thus efficacy even at very low MSLN expression levels on the treated tumor cells. To challenge this prediction, biodistribution of BAY 2287411 was evaluated in HT29-MSLN and OVCAR-3 models at three different total antibody doses ranging from 0.029 to 0.14 and 0.75 mg/kg. Specific tumor accumulation over the course of three weeks was observed in the transfected HT29-MSLN model with high MSLN expression and only minor differences in radioactivity profiles in tumors between the administered total antibody doses were observed (Supplementary Fig. S4G; Fig. 4C). Using the OVCAR-3 xenograft model with intermediate MSLN expression level (Supplementary Fig. S4H), a slightly lower accumulation in tumors was observed at the dose of 0.75 mg/kg, compared to the dose of 0.14 mg/kg. These findings are in line with the expectations from the pharmacokinetic/pharmacodynamic model which predicts a decline in accumulated thorium-227 hits per cell at

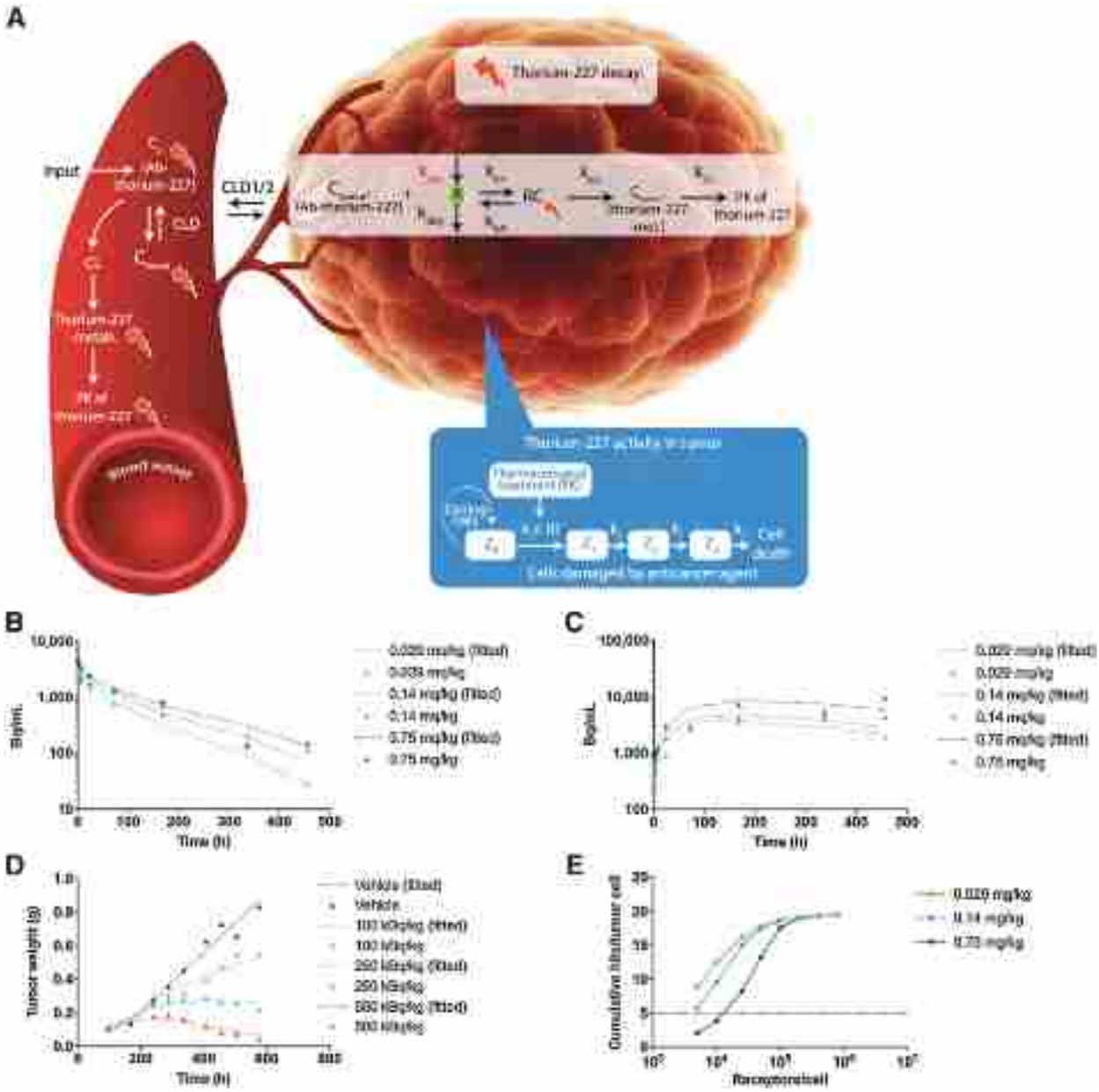

Figure 4.

Applying a pharmacokinetic/pharmacodynamic model to fit and simulate experimental data from the HT29-MSLN xenograft model. **A,** Mechanistic pharmacokinetic/pharmacodynamic model describing pharmacokinetics and pharmacodynamics of BAY 2287411. Ab, antibody; CL, conjugate blood clearance; CLD, conjugate distribution clearance (from blood to tissue); CLD1, conjugate distribution clearance (from blood to tumor); R, receptor; k_{syn}, receptor synthesis rate; k_{deg}, receptor degradation rate; k_{on}, association rate constant; k_{off}, dissociation rate constant; k_{int}, internalization rate of conjugate drug complex (RC); k_{31}, transfer rate constant of Th metabolites (tumor to plasma); k_2, potency value; k_1, transfer rate. **B** and **C,** Observed (symbols) and fitted (lines) thorium-227-radioactivity in blood (**B**) and tumor (**C**) after intravenous bolus administration of 0.029, 0.14, and 0.75 mg/kg to tumor-bearing mice (HT29-MSLN). The radioactivity dose was constant and amounted to 500 kBq/kg. **D,** Observed (symbols) and fitted (lines) tumor weight (g) after intravenous administration of 100, 250, and 500 kBq/kg to tumor-bearing female nu/nu NMRI mice. The total antibody dose was 0.14 mg/kg. **E,** Simulated cumulative hits/tumor cell over a time period of 0 to 6 weeks after intravenous administration of 0.030 to 0.75 mg/kg at a fixed radioactivity and target densities between 5,000 and 800,000 receptors/cell.

increasing total antibody doses. However, due to the rather small differences in tumor exposure, similar tumor growth inhibition was observed at both tested total antibody doses at a fixed radioactivity dose of 250 kBq/kg (Fig. 2D).

Discussion

The specific overexpression of mesothelin (MSLN) in solid tumors, combined with its restricted expression in healthy organs,

Table 2. Summary of determined tumor doubling times, potency (k_2), and TSCs in various xenograft models

Model	Assumed target density (antibodies bound/cell)	Doubling time in days[a]	k_2 (mL/Bq/h)	TSC (Bq/mL)
HT29-MSLN	242,413	3.2	2.26×10^{-6}	4,069
BxPC-3	4,200	6.1	2.11×10^{-6}	2,238
OVCAR-3	37,877	6.9	1.05×10^{-6}	3,967
ST2185B (PDX)	181,000[b]	7.1	1.28×10^{-6}	3,189
ST103 (PDX)	192,000[b]	20.3	1.13×10^{-6}	1,215
Capan-2	18,000	21	1.65×10^{-6}	838

Abbreviation: k_2, potency parameter.
[a]The tumor doubling time was calculated from the exponential tumor growth rate.
[b]Determined theoretically by extrapolation using HT29-MSLN xenograft values.

has identified it as a promising antigen for targeted cancer therapies. Several MSLN-targeting modalities ranging from antibodies, immunotoxins, ADCs, CAR T-cells, bispecific T-cell engager formats as well as vaccines (14, 16) are in preclinical and clinical development and have shown early signs of clinical efficacy. Still, mesothelioma as well as ovarian cancer remains a devastating disease of current high unmet medical need (29, 30). Therefore, the development of novel modalities offering new treatment opportunities to patients is constantly needed. We describe herein, the preclinical efficacy of a MSLN-targeted thorium-227 conjugate (BAY 2287411) comprising the fully human IgG1 antibody BAY 86-1903, covalently conjugated to a 3,2-HOPO chelator (4, 5) enabling stable complexation of the alpha particle emitter thorium-227. The radiolabeling is high yielding and robust and can be performed by simply mixing the conjugate with thorium-227 at ambient temperature. The resulting drug product formulation has been shown to be stable as evidenced by maintenance of biophysical integrity and binding properties at the 48 h timepoint post-reconstitution. The *in vivo* activity of BAY 2287411 was explored in several CDX and PDX models of colorectal, ovarian, pancreatic, breast, and lung cancer. The MoA of BAY 2287411 involves multiple pathways and cellular responses including the induction of irreparable double-strand DNA breaks, increase in oxidative stress, induction of G_2–M cell-cycle arrest, and activation of apoptotic and necrotic pathways resulting in potent cytotoxicity. Interestingly, inhibition of either apoptotic or necrotic pathways still led to decreased cellular viability, indicating involvement of potential other cell death pathways. Deficiency in homologous recombination repair, for example, *BRCA1* deletion, led to slightly higher sensitivity to BAY 2287411 in the isogenic UWB1-289 cell line pair. These MoA characteristics distinguish BAY 2287411 from other MSLN-targeting therapeutics currently in (pre)clinical development. As such, combination of BAY 2287411 with inhibitors of the DNA damage response (DDR) pathway could sensitize tumors to targeted alpha therapy. Indeed, preclinical studies are currently under investigation to evaluate the combination of TTCs with DDR inhibitors (31). In addition, due to the physical damage caused by the high energy alpha-particle tracking through the cancer cell, we also present evidence that exposure of cells to BAY 2287411 results in the induction of DAMPs, the hallmarks of immunogenic cell death (ICD). Potential stimulation of ICD may therefore be indicative of an additional contribution to MoA arising from immune system activation (26, 32). This observation has been previously reported for the alpha-emitter radium-223 dichloride (Xofigo) *in vitro* (33) and is further supported by the fact that the alpha-emitter bismuth-213 stimulated the immune system in immunocompetent mice using an *in vitro* vaccination approach (34, 35). Therefore, follow-up studies to explore the potential immunostimulatory effect of BAY 2287411 to induce immunogenic cell death *in vitro* as well as *in vivo* studies in immunocompetent mice are warranted and may support future combination studies with immune checkpoint inhibitors.

The high linear energy transfer of the alpha particle and the complex nature of the cellular damage would appear to be reflected in the significant *in vivo* efficacy of BAY 2287411 observed in the broad range of MSLN-expressing tumor models presented in this study. Indeed, this finding was supported by pharmacokinetic/pharmacodynamic modeling, which determined the potency parameter k_2 for BAY 2287411 to be in the range of 2×10^{-6} mL/Bq/h across the different *in vivo* xenograft models performed. This also indicates that the intrinsic cell killing ability of alpha radiation may not be cell-type specific, rather related to the efficiency of payload delivery and antigen expression levels, the key drivers of accumulation and tumor retention. Interestingly, in the models presented, BAY 2287411 administered as multiple doses had the same antitumor efficacy as the equivalent single dose at the study endpoint. However, the onset of tumor growth inhibition was more rapid for the single, high dose group (500 kBq/kg) indicating that a high initial absorbed dose delivered quickly to the tumor may be advantageous. This would be particularly relevant in cases where the tumor has a rapid doubling rate as supported by the data and the pharmacokinetic/pharmacodynamic predictions. The toxicological findings of BAY 2287411 generally indicated that the TTC was well-tolerated in mice based on body weight measurements and the reversibility of white blood cell suppression observed during the course of the study. These observations have been confirmed by preclinical safety studies in monkeys (data not shown).

The retention and efficacy of thorium-227 activity in tumors correlated well with MSLN expression levels. As such, the tumor regressions induced by BAY 2287411 were observed in *in vivo* models for which H-scores for MSLN were >90; for example, approximately 25% of cells staining 2+ (OVCAR-3 and Capan-2 models). Below this threshold, tumor stasis was observed as highlighted in the BxPC-3 model with an H-score of 48 in which only 7% of cells were scored 2+. This demonstrates that BAY 2287411 can be delivered highly specifically to MSLN-expressing tumor sites. However, the inherent properties of alpha emitters, such as their capability to penetrate 2 to 10 cell layers (10) and the potential to affect cells outside the direct radiation field (36) which can be particularly useful in tumors with heterogeneous target expression, might be of advantage for BAY 2287411 in comparison with other targeted therapies such as ADCs, which in contrast require high and homogeneous target expression to allow internalization and subsequent release of the toxophor. Although ADCs can be engineered with cleavable, cell-permeable payloads, initial ADC internalization remains the rate-limiting step. In addition, the potency of either bispecific T-cell engager (BiTE) constructs or CAR-T cells depends on guiding the T cell to antigen-positive tumor cells. Bystander effects for BiTEs have therefore been reported to be dependent on proximity of the cytotoxic T cell to the target-negative tumor cell (37). Indeed, when *in vivo* activity of BAY 2287411 was tested in tumor models with varying target heterogeneity, *in vivo* activity was observed at H-scores as low as 25 and 80. More work remains to determine whether this effect is

related to bystander, cross-fire or simply enhanced permeability and retention effects (38, 39). A further advantage of BAY 2287411 is its capability to overcome cellular resistance mechanisms to existing therapies. Indeed, in additional preclinical models, increased activity of BAY 2287411 over existing therapies for mesothelioma and ovarian cancer was observed (data not shown). Interestingly, and in line with a study showing that MSLN expression is recycled to the surface within 48 h after treatment (18), it was observed that MSLN expression was still detectable in BAY 2287411-treated tumors up to 54 days post-dosing.

As the number of cumulative hits per tumor cell is a function of total antibody dose and receptor density, we further investigated at which total antibody doses optimal cumulative hits can be achieved at a fixed radioactivity dose using our pharmacokinetic/pharmacodynamic model. MSLN expression levels in the range of approximately 37,877 (OVCAR-3) to 242,413 (HT29-MSLN) antibodies bound per cell and a total antibody dose of 0.14 to 0.75 mg/kg were found to be sufficient for maintaining an adequate amount of cumulative hits per tumor cell to achieve efficacy (27, 28). Interestingly, these findings are in alignment with imaging studies of two MSLN-targeting antibodies in patients for which an optimal total antibody dose of 10 to 50 mg/patient (equaling a total antibody dose of 0.14–0.71 mg/kg for a 70-kg patient) was proposed (40, 41). At total antibody doses below 10 mg/patient, tumor lesion accumulation might be negatively influenced by nonlinear pharmacokinetics due to faster clearance. In fact, slightly lower tumor accumulation of BAY 2287411 was also observed in our study when BAY 2287411 was administered at a total antibody dose of 0.029 mg/kg.

Thorium-227 has a half-life of 18.7 days and therefore, depending on the pharmacokinetics of the antibody, the maximum energy is deposited in tumors over the course of one decay. This can be experimentally observed in the biodistribution studies in which a maximum level of accumulation in mice is reached at seven days post-administration. Furthermore, it was observed that the activity was retained in the tumor up to 28 days, which might be attributed to the fact that BAY 2287411 is internalized into the cell after binding to MSLN (17). As expected, efficacy and the TSC are dependent on tumor doubling time, e.g., more pronounced efficacy was seen in the ST103 PDX model (doubling time: 20.3 days) as compared to the HT29-MSLN model (doubling time 3.2 days). Therefore, the efficacy in preclinical models is not only dependent on the MSLN-driven retention of BAY 2287411 in the tumor but also on the tumor doubling time. Hence, tumors with slower tumor doubling times may be preferred to achieve the best responses *in vivo*.

In conclusion, the preclinical data presented herein for BAY 2287411 support the future development of this TAT for the treatment of MSLN-expressing tumors, and to this end, a clinical trial application has been initiated (NCT03507452).

Disclosure of Potential Conflicts of Interest

H. Hennekes and immediate family members hold ownership interest (including patents) in Bayer AG. D. Mumberg holds ownership interest (including patents) in Bayer AG. K. Ziegelbauer holds ownership interest (including patents) in Bayer AG. No potential conflicts of interest were disclosed by the other authors.

Authors' Contributions

Conception and design: U.B. Hagemann, J. Schuhmacher, A. Kristian, J. Karlsson, R.M. Bjerke, K. Ziegelbauer, A.S. Cuthbertson

Development of methodology: U.B. Hagemann, J. Schuhmacher, V. Cruciani, S. Golfier, R. Smeets, S. Uran, J. Karlsson, O.B. Ryan, A.S. Cuthbertson

Acquisition of data (provided animals, acquired and managed patients, provided facilities, etc.): U.B. Hagemann, C. Ellingsen, A. Kristian, A. Mobergslien, V. Cruciani, K. Wickstroem, C.A. Schatz, C. Kneip, S. Golfier, R. Smeets, R.M. Bjerke

Analysis and interpretation of data (e.g., statistical analysis, biostatistics, computational analysis): U.B. Hagemann, C. Ellingsen, J. Schuhmacher, A. Kristian, C.A. Schatz, S. Uran, J. Karlsson, A.S. Cuthbertson

Writing, review, and/or revision of the manuscript: U.B. Hagemann, C. Ellingsen, J. Schuhmacher, A. Kristian, V. Cruciani, K. Wickstroem, C.A. Schatz, R. Smeets, S. Uran, H. Hennekes, J. Karlsson, R.M. Bjerke, D. Mumberg, A.S. Cuthbertson

Administrative, technical, or material support (i.e., reporting or organizing data, constructing databases): U.B. Hagemann, C. Ellingsen, K. Wickstroem, S. Uran, O.B. Ryan, A.S. Cuthbertson

Study supervision: U.B. Hagemann, R.M. Bjerke, D. Mumberg, A.S. Cuthbertson

Acknowledgments

Aurexel Life Sciences Ltd. (www.aurexel.com) is acknowledged for editorial support funded by Bayer AG. The authors thank Minerva Imaging (Copenhagen, Denmark) for excellent execution of the PDX models, delivered through START (Houston, TX). They further thank Pharmatest (Turku, Finland) and Biotest Facility (Copenhagen, Denmark) for excellent execution of cell line–derived xenograft studies. The authors thank Jochen Hilbig, Manuela Steinbach, Claudia Kamfenkel, and Manuela Brand for excellent technical support.

The costs of publication of this article were defrayed in part by the payment of page charges. This article must therefore be hereby marked *advertisement* in accordance with 18 U.S.C. Section 1734 solely to indicate this fact.

Received October 24, 2018; revised March 25, 2019; accepted May 2, 2019; published first May 7, 2019.

References

1. Targeted Alpha Therapy Working Group, Parker C, Lewington V, Shore N, Kratochwil C, Levy M, et al. Targeted alpha therapy, an emerging class of cancer agents: A review. JAMA Oncol 2018;4:1765–72.
2. Parker C, Nilsson S, Heinrich D, Helle SI, O'Sullivan JM, Fossa SD, et al. Alpha emitter radium-223 and survival in metastatic prostate cancer. N Engl J Med 2013;369:213–23.
3. Abou DS, Ulmert D, Doucet M, Hobbs RF, Riddle RC, Thorek DL. Whole-body and microenvironmental localization of radium-223 in naive and mouse models of prostate cancer metastasis. J Natl Cancer Inst 2016;108.
4. Ramdahl T, Bonge-Hansen HT, Ryan OB, Larsen S, Herstad G, Sandberg M, et al. An efficient chelator for complexation of thorium-227. Bioorg Med Chem Lett 2016;26:4318–21.
5. Deblonde G, Lohrey T, Booth C, Carter K, Parker B, Larsen A, et al. Solution thermodynamics and kinetics of metal complexation with a hydroxypyridinone chelator designed for thorium-227 targeted alpha therapy. Inorg Chem 2018;57:14337–46.
6. Dahle J, Borrebaek J, Jonasdottir TJ, Hjelmerud AK, Melhus KB, Bruland OS, et al. Targeted cancer therapy with a novel low-dose rate alpha-emitting radioimmunoconjugate. Blood 2007;110:2049–56.
7. Hagemann UB, Wickstroem K, Wang E, Shea AO, Sponheim K, Karlsson J, et al. In vitro and in vivo efficacy of a novel CD33-targeted thorium-227 conjugate for the treatment of acute myeloid leukemia. Mol Cancer Ther 2016;15:2422–31.
8. Hagemann UB, Mihaylova D, Uran SR, Borrebaek J, Grant D, Bjerke RM, et al. Targeted alpha therapy using a novel CD70 targeted thorium-227

conjugate in *in vitro* and *in vivo* models of renal cell carcinoma. Oncotarget 2017;8:56311–26.
9. Graf F, Fahrer J, Maus S, Morgenstern A, Bruchertseifer F, Venkatachalam S, et al. DNA double strand breaks as predictor of efficacy of the alpha-particle emitter Ac-225 and the electron emitter Lu-177 for somatostatin receptor targeted radiotherapy. PLoS One 2014;9:e88239.
10. Dekempeneer Y, Keyaerts M, Krasnigi A, Puttemans J, Muyldermans S, Lahoutte T, et al. Targeted alpha therapy using short-lived alpha-particles and the promise of nanobodies as targeting vehicle. Expert Opin Bio Ther 2016;16:1035–47.
11. Bera TK, Pastan I. Mesothelin is not required for normal mouse development or reproduction. Mol Cell Biol 2000;20:2902–6.
12. Chen SH, Hung WC, Wang P, Paul C, Konstantopoulos K. Mesothelin binding to CA125/MUC16 promotes pancreatic cancer cell motility and invasion via MMP-7 activation. Sci Rep 2013;3:1870.
13. Rump A, Morikawa Y, Tanaka M, Minami S, Umesaki N, Takeuchi M, et al. Binding of ovarian cancer antigen CA125/MUC16 to mesothelin mediates cell adhesion. J Biol Chem 2004;279:9190–8.
14. Morello A, Sadelain M, Adusumilli PS. Mesothelin-targeted CARs: driving T cells to solid tumors. Cancer Discov 2016;6:133–46.
15. Bharadwaj U, Marin-Muller C, Li M, Chen C, Yao Q. Mesothelin confers pancreatic cancer cell resistance to TNF-alpha-induced apoptosis through Akt/PI3K/NF-kappaB activation and IL-6/Mcl-1 overexpression. Mol Cancer 2011;10:106.
16. Zhao XY, Subramanyam B, Sarapa N, Golfier S, Dinter H. Novel antibody therapeutics targeting mesothelin in solid tumors. Clin Cancer Drugs 2016;3:76–86.
17. Golfier S, Kopitz C, Kahnert A, Heisler I, Schatz CA, Stelte-Ludwig B, et al. Anetumab ravtansine: a novel mesothelin-targeting antibody-drug conjugate cures tumors with heterogeneous target expression favored by bystander effect. Mol Cancer Ther 2014;13:1537–48.
18. Quanz M, Hagemann U, Zitzmann-Kolbe S, Stelte-Ludwig B, Golfier S, Elbi C, et al. Anetumab ravtansine inhibits tumor growth and shows additive effect in combination with targeted agents and chemotherapy in mesothelin-expressing human ovarian cancer models. Oncotarget 2018;9:34103–21.
19. DelloRusso C, Welcsh PL, Wang W, Garcia RL, King MC, Swisher EM. Functional characterization of a novel BRCA1-null ovarian cancer cell line in response to ionizing radiation. Mol Cancer Res 2007;5:35–45.
20. Lindmo T, Boven E, Cuttitta F, Fedorko J, Bunn PA, Jr. Determination of the immunoreactive fraction of radiolabeled monoclonal antibodies by linear extrapolation to binding at infinite antigen excess. J Immunol Methods 1984;72:77–89.
21. Baidoo KE, Yong K, Brechbiel MW. Molecular pathways: targeted alpha-particle radiation therapy. Clin Cancer Res 2013;19:530–7.
22. Goldstein JC, Munoz-Pinedo C, Ricci JE, Adams SR, Kelekar A, Schuler M, et al. Cytochrome c is released in a single step during apoptosis. Cell Death Differ 2005;12:453–62.
23. Jiang X, Wang X. Cytochrome C-mediated apoptosis. Annu Rev Biochem 2004;73:87–106.
24. Azzam EI, Jay-Gerin JP, Pain D. Ionizing radiation-induced metabolic oxidative stress and prolonged cell injury. Cancer Lett 2012;327:48–60.
25. Degterev A, Maki JL, Yuan J. Activity and specificity of necrostatin-1, small-molecule inhibitor of RIP1 kinase. Cell Death Differ 2013;20:366.
26. Bezu L, Gomes-de-Silva LC, Dewitte H, Breckpot K, Fucikova J, Spisek R, et al. Combinatorial strategies for the induction of immunogenic cell death. Front Immunol 2015;6:187.
27. Sgouros G, Roeske JC, McDevitt MR, Palm S, Allen BJ, Fisher DR, et al. MIRD Pamphlet No. 22 (Abridged): Radiobiology and dosimetry of alpha-particle emitters for targeted radionuclide therapy. J Nucl Med 2010;51:311–28.
28. Bird RP, Rohrig N, Colvett RD, Geard CR, Marino SA. Inactivation of synchronized Chinese hamster V79 cells with charged-particle track segments. Radiat Res 1980;82:277–89.
29. Christoph DC, Eberhardt WE. Systemic treatment of malignant pleural mesothelioma: new agents in clinical trials raise hope of relevant improvements. Curr Opin Oncol 2014;26:171–81.
30. Herzog TJ, Monk BJ. Bringing new medicines to women with epithelial ovarian cancer: what is the unmet medical need? Gynecol Oncol Res Pract 2017;4.
31. Wickstroem K, Hagemann UB, Cruciani V, Wengner AM, Kristian A, Ellingsen C, et al. Synergistic Effect of a Mesothelin Targeted Thorium-227 Conjugate in Combination with DNA Damage Response Inhibitors in Ovarian Cancer Xenograft Models. J Nucl Med 2019 Mar 8. [Epub ahead of print].
32. Vatner RE, Cooper BT, Vanpouille-Box C, Demaria S, Formenti SC. Combinations of immunotherapy and radiation in cancer therapy. Front Oncol 2014;4:325.
33. Malamas AS, Gameiro SR, Knudson KM, Hodge JW. Sublethal exposure to alpha radiation (223Ra dichloride) enhances various carcinomas' sensitivity to lysis by antigen-specific cytotoxic T lymphocytes through calreticulin-mediated immunogenic modulation. Oncotarget 2016;7:86937–47.
34. Gorin JB, Guilloux Y, Morgenstern A, Cherel M, Davodeau F, Gaschet J. Using alpha radiation to boost cancer immunity? Oncoimmunology 2014;3:e954925.
35. Gorin JB, Menager J, Gouard S, Maurel C, Guilloux Y, Faivre-Chauvet A, et al. Antitumor immunity induced after alpha irradiation. Neoplasia 2014;16:319–28.
36. Marin A, Martin M, Linan O, Alvarenga F, López M, Fernández L, et al. Bystander effects and radiotherapy. Rep Pract Oncol Radiother 2015;20:12–21.
37. Ross SL, Sherman M, McElroy PL, Lofgren JA, Moody G, Baeuerle PA, et al. Bispecific T cell engager (BiTE) antibody constructs can mediate bystander tumor cell killing. PLoS One 2017;12:e0183390.
38. Maeda H, Nakamura H, Fang J. The EPR effect for macromolecular drug delivery to solid tumors: Improvement of tumor uptake, lowering of systemic toxicity, and distinct tumor imaging in vivo. Adv Drug Deliv Rev 2013;65:71–9.
39. Matsumura Y, Maeda H. A new concept for macromolecular therapeutics in cancer chemotherapy: mechanism of tumoritropic accumulation of proteins and the antitumor agent smancs. Cancer Res 1986;46(12 Pt 1):6387–92.
40. Lamberts LE, Menke-van der Houven van Oordt CW, ter Weele EJ, Bensch F, Smeenk MM, Voortman J, et al. ImmunoPET with anti-mesothelin antibody in patients with pancreatic and ovarian cancer before anti-mesothelin antibody-drug conjugate treatment. Clin Cancer Res 2016;22:1642–52.
41. Lindenberg L, Thomas A, Adler S, Mena E, Kurdziel K, Maltzman J, et al. Safety and biodistribution of 111In-amatuximab in patients with mesothelin expressing cancers using single photon emission computed tomography-computed tomography (SPECT-CT) imaging. Oncotarget 2015;6:4496–504.
42. Barretina J, Caponigro G, Stransky N, Venkatesan K, Margolin AA, Kim S, et al. The Cancer Cell Line Encyclopedia enables predictive modelling of anticancer drug sensitivity. Nature 2012;483:603–7.
43. Garnett MJ, Edelman EJ, Heidorn SJ, Greenman CD, Dastur A, Lau KW, et al. Systematic identification of genomic markers of drug sensitivity in cancer cells. Nature 2012;483:570–5.